

Linearization of friction effects in vibration of two rotating blades

M. Byrtus^{a,*}, M. Hajžman^a, V. Zeman^a

^aFaculty of Applied Sciences, University of West Bohemia, Univerzitní 22, 306 14 Plzeň, Czech Republic

Received 6 November 2009; received in revised form 27 June 2013

Abstract

This paper is aimed at modelling of friction effects in blade shrouding which are realized by means of friction elements placed between blades. In order to develop a methodology of modelling, two blades with one friction element in between are considered only. Flexible blades fixed to a rotating disc are discretized by FEM using 1D Rayleigh beam elements derived in rotating space as well as the friction element modelled as a rigid body. The blades and the friction element are connected through two concurrent friction planes, where the friction forces arise on the basis of centrifugal force acting on the friction element. The linearization of friction is performed using the harmonic balance method to determine equivalent damping coefficients in dependence on the amplitudes of relative slip motion between the blades and the friction element. The methodology is applied to a model of two real blades and will be extended for the whole bladed disc with shrouding.

© 2013 University of West Bohemia. All rights reserved.

Keywords: bladed disc, friction, harmonic balance method, damping

1. Introduction

Blades are the common and the most important elements in turbine design. With the increase of an energy consumption turbines are still innovated and the power of developed turbines is growing. On the other hand it brings the greater complexity of newly produced energy systems and higher requirements on blades strength and fatigue. Even if a machine is properly designed with respect to excitation frequencies and turbine eigenfrequencies, some excitation sources cannot be included in preliminary developments. Therefore the blades should be designed in such a way that they can absorb vibrations caused by unexpected or unusual excitation. Mathematical and computational models of blades and their systems are suitable tools for the investigation of their dynamical properties and for their optimization.

One of the most usual approaches to the suppression of undesirable blade vibrations is the employment of various friction effects. Detailed investigation of influences of friction on dynamical response of a simplified mechanical system represented by a beam can be found in [4]. Mainly the microslip phenomenon is discussed. Another method, which is analytical one and is connected with non-spherical geometries, is developed in [1]. Many publications deal with the friction induced by means of underplatform (wedge) dampers. A method for the calculation of static balance supposing an in-plane motion of the wedge dampers is developed in [6]. An analytical approach is described in [2] and comparison of numerical simulation results with the results obtained by linearization is shown in [5]. The harmonic balance method for the evaluation of friction effects in blade dynamics represented by a very simple discrete mechanical system is discussed in [3]. Also experimental methods for the evaluation of friction significance

*Corresponding author. Tel.: +420 377 632 315, e-mail: mbyrtus@kme.zcu.cz.

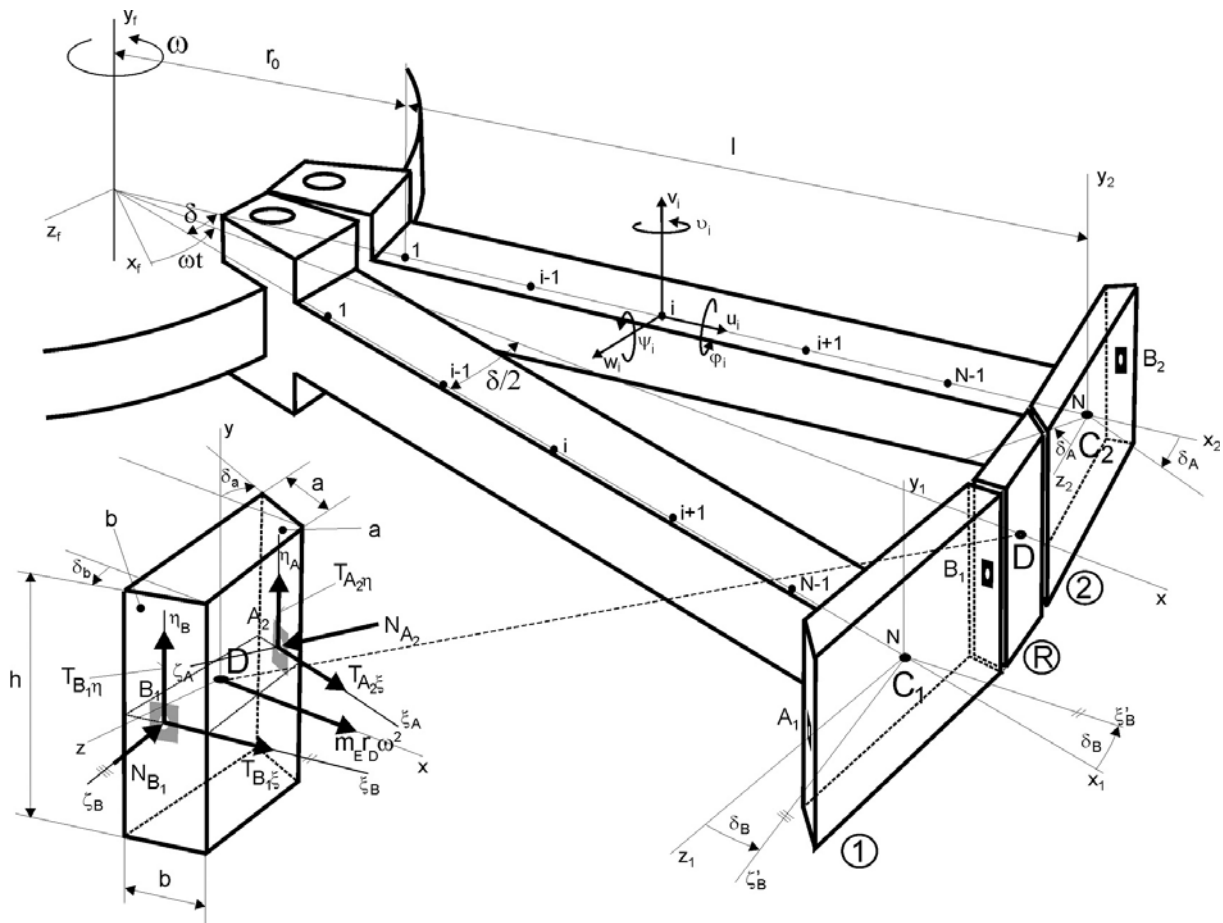


Fig. 1. Two rotating blades with a friction element

in the problems of blade vibrations are very important. Some comparison of experimental and theoretical analysis is shown in [15], pure experimental results are described in [14] and the influences of temperature are experimentally investigated in [13].

This paper deals with the modelling and dynamical analysis of a spatial system of two adjacent flexible blades with rigid shroud and one friction element, which is placed in shroud. The dynamic analysis approach is based on the harmonic balance method to replace the nonlinear friction forces with linear viscous forces determined by equivalent damping coefficients.

2. Modelling of two blades with friction coupling in rotating space

Let us consider a rigid disc with flexible blades which rotates with constant angular velocity ω in a fixed space x_f, y_f, z_f . The blade roots are fixed to the disc and every two adjacent blades are connected by means of a friction element which is wedged between the blade shrouds (see Fig. 1). As the blades rotate, the centrifugal force pushes the element towards contact surfaces a and b of the adjacent blade shroud and normal forces at the contact patches increase. Consequently, larger friction forces act on shroud in case of slip motion between the shroud and the friction element.

2.1. Rigid body

First, let us derive equations of motion of a rigid body in coordinate space x, y, z rotating with constant angular velocity ω around fixed axis y_f . The position of the body is described in rotating coordinate space x, y, z by three displacements u, v, w of the gravity centre C and

where M_B , B_B , $K_{s,B}$ are symmetrical mass, material damping and stiffness matrices, respectively. Matrix G_B is skew-symmetrical and expresses gyroscopic effects. These matrices are assembled in local configuration space of the blade rotating around axis y_f with longitudinal axis x_j ($j = 1, 2$) defined by vector of generalized coordinates $q_B \in \mathbb{R}^{6N}$ having following structure

$$q_B = [\dots u_i, v_i, w_i, \varphi_i, \vartheta_i, \psi_i, \dots]^T, \quad i = 1, \dots, N, \quad (5)$$

where u_i, v_i, w_i are translational and $\varphi_i, \vartheta_i, \psi_i$ are rotational displacements of the blade in node i (see Fig. 1). Matrix $K_{d,B}$ is matrix of softening under rotation and $K_{\omega,B}$ is matrix of bending stiffening that expresses the influence of resistance in bending produced by centrifugal forces acting on the blade. The force vector $f_{\omega,B}$ describes centrifugal forces acting on blade elements at their nodes.

The model of the shroud is included in matrices M_B , G_B and $K_{d,B}$ where mass, gyroscopic and stiffness matrices of the shroud presented in (3) are added on positions corresponding to coordinates of the nodal point N . Similarly, vector $f_{\omega,B}$ of centrifugal forces is modified and the centrifugal force acting on the shroud modelled as a rigid body is added on position corresponding to the mentioned nodal coordinates.

2.3. Model of blade couple with friction element

Here, the model of two adjacent blades interconnected by a friction element will be introduced (Fig. 1). Based on previous sections, corresponding mathematical model can be written in generalized rotating coordinate system defined by vector $q = [q_1^T, q_R^T, q_2^T]^T \in \mathbb{R}^{6(N_1+1+N_2)}$ in following form

$$M\ddot{q} + (\omega G + B + B_C)\dot{q} + (K_s - \omega^2 K_d + \omega^2 K_\omega + K_C)q + h(\dot{q}) = f_\omega. \quad (6)$$

Mass, damping and stiffness matrices are arranged using models of the blades and the rigid body. Matrices in (6) are block diagonal and have this structure

$$\begin{aligned} M &= \text{diag} (M_1, M_R, M_2), \quad G = \text{diag} (G_1, G_R, G_2), \\ B &= \text{diag} (B_1, \mathbf{0}, B_2), \quad K_s = \text{diag} (K_{s,1}, \mathbf{0}, K_{s,2}), \\ K_d &= \text{diag} (K_{d,1}, K_{d,R}, K_{d,2}), \quad K_\omega = \text{diag} (K_{\omega,1}, \mathbf{0}, K_{\omega,2}), \end{aligned} \quad (7)$$

where indices 1 and 2 designate the first and the second blade, respectively. The index R corresponds to the friction element, which is modeled as a rigid body. The vector of excitation has the form $f_\omega = [f_{\omega,1}^T, f_{\omega,R}^T, f_{\omega,2}^T]^T$. The mathematical model (6) includes moreover coupling stiffness matrix K_C and the vector $h(\dot{q})$, which express stiffness effects and nonlinear friction forces in friction couplings between the shroud of blade 1 and 2 and the friction element R , respectively. Damping matrix proportional to contact stiffness matrix $B_C = \beta_C K_C$ comprises the influence of contact damping in contact surfaces.

2.3.1. Coupling stiffness determination

Let us deal with force effects arising in contact patches between the shroud and the friction element. The friction element has two contact surfaces a and b . At geometrical centers B_1 and A_2 of the surfaces, coordinate systems ξ_B, η_B, ζ_B and ξ_A, η_A, ζ_A are placed in such a way, that planes $\xi_B \eta_B$ and $\xi_A \eta_A$ coincide with surfaces a and b , respectively, and axes ζ_B and ζ_A are perpendicular to them (see Fig. 1, left bottom). In these coordinate systems, the forces acting

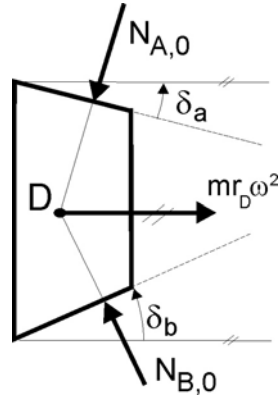


Fig. 3. Forces acting on friction element

on the friction element at point B_1 (A_2) can be expressed using normal force N_{B_1} (N_{A_2}) and friction forces $T_{B_1\xi}$ and $T_{B_1\eta}$ ($T_{A_2\xi}$ and $T_{A_2\eta}$). The resultant normal forces can be written as

$$N_{B_1} = N_{B,0} - k_b (\xi_{B,C_1}^T \mathbf{q}_{C_1} - \xi_{B,D}^T \mathbf{q}_D), \quad N_{A_2} = N_{A,0} + k_a (\xi_{A,C_2}^T \mathbf{q}_{C_2} - \xi_{A,D}^T \mathbf{q}_D), \quad (8)$$

where $N_{B,0}$ and $N_{A,0}$ are magnitudes of normal forces resulting from equilibrium conditions of non-vibrating friction element

$$N_{A,0} = mr_D \omega^2 \frac{\cos \delta_b}{\sin(\delta_a + \delta_b)}, \quad N_{B,0} = mr_D \omega^2 \frac{\cos \delta_a}{\sin(\delta_a + \delta_b)}. \quad (9)$$

Angles δ_a and δ_b describe friction element skewing (see Fig. 3). Parameters k_b and k_a express translational contact stiffnesses of contact patches and their linearized magnitudes are expressed according to

$$k_a = \frac{N_{A,0}}{\gamma_a} \cdot 10^6 [\text{N/m}], \quad k_b = \frac{N_{B,0}}{\gamma_b} \cdot 10^6 [\text{N/m}]. \quad (10)$$

Symbols γ_a and γ_b designate surface contact deformation in micrometers and are defined as follows [12]

$$\gamma_a = c\sigma_a^p, \quad \gamma_b = c\sigma_b^p, \quad (11)$$

where c is contact deformation coefficient, p is contact power index and σ_a , σ_b express average contact pressure. According to contact pressure definition, in case of neglecting of vibration influence it holds

$$\sigma_a = \frac{N_{A,0}}{A_{ef,a}}, \quad \sigma_b = \frac{N_{B,0}}{A_{ef,b}}, \quad (12)$$

where $A_{ef,a} = h_{ef}a_{ef}$ and $A_{ef,b} = h_{ef}b_{ef}$ designate supposed effective area of the corresponding contact surface, whose size can be estimated based on its experimentally gained wearing [10]. Vectors $\xi_{XY} \in \mathbb{R}^{6,1}$ are geometric transformation vectors which transform the blade displacements in nodal point Y described by vector \mathbf{q}_Y to a normal displacement of the contact point X at the contact surface. The terms in brackets in (8) express relative normal contact deflection between the shroud and the friction element with respect to the contact surface.

Since the blade shrouds and the friction element can rotate about their gravity center axes, it is necessary to include moreover the influence of torque in the contact surfaces. Under the assumption of identical contact stiffness in whole contact areas, the resultant torque can be

described by so called rotational contact stiffnesses of contact surfaces which are defined using the translational contact stiffnesses in following way

$$\begin{aligned} k_{xx}^{(a)} &= \frac{k_a}{12} \cos^2 \delta_a h_{ef}^2, & k_{xx}^{(b)} &= \frac{k_b}{12} \cos^2 \delta_b h_{ef}^2, & k_{yy}^{(a)} &= \frac{k_a}{12} a_{ef}^2, & k_{yy}^{(b)} &= \frac{k_b}{12} b_{ef}^2, \\ k_{zz}^{(a)} &= \frac{k_a}{12} \sin^2 \delta_a h_{ef}^2, & k_{zz}^{(b)} &= \frac{k_b}{12} \sin^2 \delta_b h_{ef}^2. \end{aligned} \quad (13)$$

Used quantities k_a and k_b are defined above as well as the meaning of angles δ_a and δ_b . The stiffnesses $k_{ax}^{(a)}$ and $k_{ax}^{(b)}$ of axial mounting of the friction element in the shroud of both blades in direction of axis y depend on the structure design. These stiffnesses influence the blade vibration very few and hinder friction element falling out. They are invariant with respect to all used coordinate systems because the axial mounting is parallel with z axes which are mutually parallel too.

Based on the above mentioned assumptions, we can express vectors of conservative forces describing mutual acting of the friction element and the blade shrouds. Because of their assumed linearity, the force vectors can be substituted by the coupling stiffness matrix presented in (6) which can be written as a sum of

$$\mathbf{K}_C = \mathbf{K}_C^{(t)} + \mathbf{K}_C^{(r)} + \mathbf{K}_C^{(ax)}, \quad (14)$$

where matrices on the right hand side describe influence of translational, rotational and axial coupling stiffnesses, respectively.

2.3.2. Friction effects determination

Now, let us deal with the nonconservative part of coupling forces. The friction forces acting on the friction element concentrated into central contact points B_1 and A_2 are nonlinear and can be expressed as

$$\vec{T}_{B_1} = f_b N_{B_1} \frac{\vec{v}_{s,B_1}}{|\vec{v}_{s,B_1}|}, \quad \vec{T}_{A_2} = f_a N_{A_2} \frac{\vec{v}_{s,A_2}}{|\vec{v}_{s,A_2}|}, \quad (15)$$

where f_b (f_a) is the friction coefficient of friction surface b (a) and \vec{v}_{s,B_1} (\vec{v}_{s,A_2}) is slip velocity of blade shroud “1” (“2”) with respect to friction element in point B_1 (A_1) expressed in $\xi_B \eta_B$ ($\xi_A \eta_A$) plane. The friction forces acting on the blade shroud have opposite direction.

To linearize the nonlinear friction forces (15) included in (6), the harmonic balance method is used. There are many linearization techniques employed in nonlinear system investigation [9]. It depends on which kind of parameters one needs to investigate and on the excitation included in the system. The aim of the linearization technique is to replace the original nonlinear system with a linear one. The method chosen here is based on following assumptions:

1. Both nonlinear friction torques and forces acting on a friction element interact mutually very weak, therefore equivalent damping coefficients can be considered independently.
2. The slip motion of friction surfaces can be simply considered as one degree of freedom motion in the direction of the slip.
3. Excitation is supposed to be a periodic function as well as the steady-state response.
4. The friction and excitation forces are expandable into a Fourier series.

Based on this, the term for determination of equivalent damping coefficient for k -th harmonic component with angular frequency ω_k [16] can be derived in following form

$$b_e(a_k, \omega_k) = \frac{4T}{\pi a_k \omega_k}, \quad (16)$$

where T is the magnitude of friction force, a_k is the amplitude of steady slip motion and ω_k is excitation angular frequency. According to known experimental observations, the term (16) does not fit real, measured amplitudes of slip motion. In [11], a modification of (16) is suggested

$$b_e(a_k, \omega_k) = \frac{4T}{\pi (a_k \omega_k)^{1.112}}. \quad (17)$$

Physically, the term $a_k \omega_k$ presents the amplitude of corresponding harmonic component of the slip velocity. Using the modified equivalent damping coefficient (17), each harmonic component of nonlinear friction forces (15) can be linearized and expressed by the coefficient of equivalent viscous translational and rotational damping (e.g. for the point B_1)

$$b_e^{(t)}(a_{B,k}^{(t)}, \omega_k) = \frac{4T}{\pi (a_{B,k}^{(t)} \omega_k)^{1.112}}, \quad b_e^{(r)}(a_{B,k}^{(r)}, \omega_k) = \frac{4M}{\pi (a_{B,k}^{(r)} \omega_k)^{1.112}}. \quad (18)$$

Variables $a_{B,k}^{(t)}$ and $a_{B,k}^{(r)}$ constitute translational and rotational slip amplitudes excited by k -th harmonic component, respectively. The linearized friction forces in (15) and friction torque M_{B_1} acting on the friction element can be then rewritten using (16) into (again for the point B_1)

$$\vec{T}_{B_1} = \frac{4T}{\pi (a_{B_1}^{(t)} \omega_0)^{1.112}} \vec{v}_{s,B_1}, \quad M_{B_1} = \frac{4M}{\pi (a_{B_1}^{(r)} \omega_0)^{1.112}} \dot{\psi}_B, \quad (19)$$

where magnitude of friction force reads $T = f_b N_{B,0}$ and providing the same contact pressure on a circular surface with radius r_{ef} , magnitude M of friction torque is $M = \frac{2}{3} f_b r_{ef} N_{B,0}$. Variable $\dot{\psi}_B$ designates relative rotational slip velocity of the blade “1” with respect to friction element in $\xi_B \eta_B$ plane, i.e. about ζ_B axis (see Fig. 2).

For illustration, ξ -component of friction force expressed in coordinate system of the friction element states as

$$T_{B_1\xi} = b(a_{B\varphi}) c_{B\xi}, \quad (20)$$

where $a_{B\xi}$ is the slip amplitude in ξ -direction and $c_{B\xi}$ represents ξ -component of slip velocity and can be expressed as

$$c_{B\xi} = \tau_{B,C_1}^T \dot{q}_{C_1} - \tau_{B,D}^T \dot{q}_D. \quad (21)$$

Quantities τ_{B,C_1}^T and $\tau_{B,D}^T$ are shown in (29).

Finally, the nonlinear mathematical model (6) can be equivalently replaced by linearized one for each excitation harmonic component with frequency ω_0

$$M\ddot{q} + (\omega G + B + B_C + B_e(\mathbf{a}, \omega_0))\dot{q} + (K_s - \omega^2 K_d + \omega^2 K_w + K_C)q = \mathbf{f}_w + \mathbf{f}(\omega_0)e^{i\omega_0 t}. \quad (22)$$

Friction torques and forces are represented by equivalent damping matrix $B_e(\mathbf{a}, \omega_0)$, where $\mathbf{a} = [a_A^{(t)}, a_A^{(r)}, a_B^{(t)}, a_B^{(r)}]^T$ is a vector containing steady slip amplitudes. Vector $\mathbf{f}(\omega_0)$ of complex amplitudes represents external harmonic excitation with frequency equal to ω_0 .

2.3.3. Equivalent damping calculation for steady-state response

Even if the terms in (18) hold, they depend on slip amplitude of the examined motion. For this purpose, it is necessary to perform any estimation of this amplitude. To approach the real slip amplitude as close as possible we use the linearized model neglecting the equivalent damping matrix. Further, let us point out, that the force vector \mathbf{f}_ω in (22) includes constant centrifugal forces in the rotating coordinate system and therefore corresponding response is a constant vector of displacements. This vector has also no influence on the equivalent damping coefficients. In the next, the influence of centrifugal forces can be neglected and the equivalent damping coefficients are calculated for harmonic excitation. To gain the global response to harmonic and centrifugal (static) excitation the superposition law for linear systems can be advantageously used.

Let us find the steady-state solution of (22) in rotating system space in complex domain in this form

$$\mathbf{q}(t) = \tilde{\mathbf{q}}(\omega_0)e^{i\omega_0 t}, \quad (23)$$

where $\tilde{\mathbf{q}}$ is a vector of complex amplitudes of displacements and $i = \sqrt{-1}$. To determine the complex amplitude, let us put (23) in (22) for $\mathbf{f}_\omega = \mathbf{0}$, $\mathbf{B}_e = \mathbf{0}$ and we obtain

$$\tilde{\mathbf{q}}(\omega_0) = [-\omega_0^2 \mathbf{M} + i\omega_0(\omega \mathbf{G} + \mathbf{B} + \mathbf{B}_C) + (\mathbf{K}_s - \omega^2 \mathbf{K}_d + \omega^2 \mathbf{K}_\omega + \mathbf{K}_C)]^{-1} \mathbf{f}(\omega_0), \quad (24)$$

where $\mathbf{f}(\omega_0)$ is vector of complex amplitudes of harmonic excitation. Based on the vector of complex amplitudes of displacements, the complex amplitudes of slip motion between contact surfaces can be determined. Let us focus on contact point B_1 . The complex translational slip amplitude in $\xi_B \eta_B$ plane can be defined as

$$\tilde{a}_B = \tilde{a}_{B\xi} + i\tilde{a}_{B\eta} = \bar{a}_{B\xi} + i\bar{\bar{a}}_{B\xi} + i(\bar{a}_{B\eta} + i\bar{\bar{a}}_{B\eta}), \quad (25)$$

where $\tilde{a}_{B\xi}$ and $\tilde{a}_{B\eta}$ are complex slip amplitudes in the direction of ξ_B and η_B axis, respectively, \bar{a} and $\bar{\bar{a}}$ denote real and complex part. The complex amplitudes are determined for contact point B_1 as follows

$$\tilde{a}_{B\xi} = \boldsymbol{\xi}_{B,C_1}^T \mathbf{q}_{C_1} - \boldsymbol{\xi}_{B,D}^T \mathbf{q}_D, \quad \tilde{a}_{B\eta} = \boldsymbol{\eta}_{B,C_1}^T \mathbf{q}_{C_1} - \boldsymbol{\eta}_{B,D}^T \mathbf{q}_D, \quad (26)$$

for contact point A_2

$$\tilde{a}_{A\xi} = \boldsymbol{\xi}_{A,C_2}^T \mathbf{q}_{C_2} - \boldsymbol{\xi}_{A,D}^T \mathbf{q}_D, \quad \tilde{a}_{A\eta} = \boldsymbol{\eta}_{A,C_2}^T \mathbf{q}_{C_2} - \boldsymbol{\eta}_{A,D}^T \mathbf{q}_D \quad (27)$$

and complex rotational slip amplitudes

$$\tilde{a}_{A\varphi} = \boldsymbol{\tau}_{A,C_2}^T \mathbf{q}_{C_2}^{(r)} - \boldsymbol{\tau}_{A,D}^T \mathbf{q}_D^{(r)}, \quad \tilde{a}_{B\varphi} = \boldsymbol{\tau}_{B,C_2}^T \mathbf{q}_{C_2}^{(r)} - \boldsymbol{\tau}_{B,D}^T \mathbf{q}_D^{(r)}. \quad (28)$$

Transformation vectors $\boldsymbol{\xi}_{X,Y} (\boldsymbol{\eta}_{X,Y}) \in \mathbb{R}^{6,1}$ transform the blade displacements in nodal point Y defined by vector \mathbf{q}_Y to a translational displacement in ξ (η) direction of contact point X laying in the contact surface. Vectors $\boldsymbol{\tau}_{X,Y} \in \mathbb{R}^{3,1}$ transform rotational displacements in nodal point Y described by vector $\mathbf{q}_Y^{(r)}$ to rotational displacements in contact point X . Transformation vectors

have following structure

$$\begin{aligned}
 \xi_{B,C_1}^T &= [\sin \delta_B, 0, \cos \delta_B, 0, -\overline{BC}_1 \sin \delta_B, 0], \\
 \xi_{B,D}^T &= [\sin \delta_b, 0, \cos \delta_b, 0, \overline{BD} \sin \delta_b, 0], \\
 \eta_{B,C_1}^T &= [0, 1, 0, \overline{BC}_1, 0, 0], \\
 \eta_{B,D}^T &= [0, 1, 0, -\overline{BD}, 0, 0], \\
 \xi_{A,C_2}^T &= [-\sin \delta_A, 0, \cos \delta_A, 0, -\overline{AC}_2 \sin \delta_A, 0], \\
 \xi_{A,D}^T &= [-\sin \delta_a, 0, \cos \delta_a, 0, \overline{AD} \sin \delta_a, 0], \\
 \eta_{A,C_2}^T &= [0, 1, 0, -\overline{AC}_2, 0, 0], \\
 \eta_{A,D}^T &= [0, 1, 0, \overline{AD}, 0, 0], \\
 \tau_{A,C_2}^T &= [\cos \delta_A, 0, \sin \delta_A, 0, \overline{AC}_2 \cos \delta_A, 0], \\
 \tau_{A,D}^T &= [\cos \delta_a, 0, \sin \delta_a, 0, -\overline{AD} \cos \delta_a, 0], \\
 \tau_{B,C_1}^T &= [\cos \delta_B, 0, -\sin \delta_B, 0, -\overline{BC}_1 \cos \delta_B, 0], \\
 \tau_{B,D}^T &= [\cos \delta_b, 0, -\sin \delta_b, 0, \overline{BD} \cos \delta_b, 0].
 \end{aligned} \tag{29}$$

The subscripts of the contact point designation have been left out according to relations (25)–(29).

Using the relations (25)–(28), equivalent damping coefficients (18) can be evaluated for both contact surfaces and for each harmonic component of excitation. Instead of the amplitude of corresponding slip motion, the absolute value of complex amplitudes (25) has to be used. Expressing the vector of slip amplitudes $\mathbf{a} = [|\tilde{a}_A^{(t)}|, |\tilde{a}_A^{(r)}|, |\tilde{a}_B^{(t)}|, |\tilde{a}_B^{(r)}|]^T$ we can determine the equivalent damping matrix in (22) and evaluate the vector of complex amplitudes of displacements taking into account the linearized nonlinear friction effects.

3. Application

The methodology of the modelling presented above is used for dynamic analysis of a real blade couple (see Fig. 4). Although the real blade packet consists of five blades connected with four friction elements, the methodology is proved on one blade couple connected with one friction body. The blades are fixed to a rigid disc rotating with constant angular velocity. Detailed geometrical description of the blades was gained from [10]. Based on the derived methodology, in-house software for computational blade modelling was developed. Using this software, each blade was divided by six nodal points into five finite beam elements. Final computational model has 78 DOF (two blades and one friction body). Basic geometrical parameters (see Fig. 1) used during numerical calculations are: $b = 0.006$ m, $h = 0.02$ m, $l = 0.21$ m, $r_D = 0.4655$ m, $\delta_a = 20^\circ$, $\delta_b = 0^\circ$, weight of friction element $m = 0.0086$ kg. Parameters used for contact stiffnesses calculations $c = 3$, $p = 0.5$. Dimensions of effective contact surface are supposed to be $h_{aef} = h_{bef} = 0.016$ m, $a_{ef} = 0.0051$ m, $b_{ef} = 0.0048$ m and the friction coefficient f is varied from 0.1 to 0.3.

3.1. Modal analysis

The derived linearized model (22) is used as a first approximation of the nonlinear behaviour of the blade packet. Performing the modal analysis, we can see the influence of friction damping on the spectrum of natural frequencies.



Fig. 4. Blade packet with friction elements

Table 1. Chosen natural frequencies of blade couple — conservative model

ν	Natural frequency [Hz]			Mode shape
	0 rpm	2 000 rpm	3 000 rpm	
1	133.8	136.9	140.7	blade bending in xy plane
2	153.7	198.2	197.9	blade bending in xy plane, FE displacement
3	158.2	267.5	268.2	blade bending in xz plane
4	178.3	540.4	561.4	dominant blade torsion
5	266.8	955.8	959.7	blade bending in in xy plane
6	356.4	1 012.5	1 020.2	blade torsion
7	449.2	1 255.5	1 270.8	blade bending in xz plane
8	724.2	1 680.4	1 693.7	blade bending in xz plane
9	958.8	1 866.3	1 868.1	blade bending in xz plane
10	959.1	2 622.2	2 716.6	blade torsion
11	1 058.4	2 729.6	2 775.2	blade bending in yz plane, FE twisting about z axis
12	1 554.2	2 881.5	3 294.2	blade torsion, FE twisting about z axis

Abbreviation FE denotes Friction Element.

3.1.1. Conservative model

To gain natural frequencies and corresponding mode shapes of the conservative model, we perform the modal analysis of the model (22) where we put $\mathbf{B} = \mathbf{B}_e = \mathbf{B}_C = \mathbf{0}$. Because of the presence of matrices of softening and bending stiffening under rotation and of the matrix of gyroscopic effects in the model, natural frequencies depend on angular velocity $\omega = \pi n/30$ rad/s, where n designates rotational speed of the disc defined in revolutions per minute. The eigenvalues are complex conjugate with zero real part. Imaginary parts of chosen eigenvalues are presented in the Table 1 along with the description of corresponding mode shapes. As the disc

Table 2. Influence of friction on real parts of eigenvalues — nonconservative model

ν	Eigenvalues f_ν [Hz]				
	$f = 0$	$f = 0.1$	$f = 0.2$	$f = 0.3$	$f = 0.4$
1	$-0.6 + 136.9i$	-0.002	-0.001	-0.0007	-0.0005
2	$-1.2 + 198.8i$	-0.1	-0.05	-0.02	-0.01
3	$-2.2 + 267.5i$	$-2.7 + 188i$	$-4.3 + 188.2i$	-0.1	-0.1
4	$-9.1 + 540.2i$	$-2.4 + 267.5i$	$-2.5 + 267.5i$	$-5.9 + 188.5i$	$-7.5 + 188.9i$
5	$-28.5 + 955.4i$	$-21.4 + 594.2i$	$-31.4 + 595.5i$	$-2.7 + 267.5i$	$-2.8 + 267.5i$
6	$-32 + 1012i$	$-52 + 1001i$	$-72 + 1008i$	$-41 + 598i$	$-50.5 + 601.4i$
7	$-49 + 1254i$	$-52 + 1205i$	$-59 + 1207i$	$-89 + 1018i$	$-102 + 1031i$
8	$-88 + 1678i$	$-78 + 1562i$	$-77 + 1562i$	$-65 + 1209i$	$-71 + 1213i$
9	$-109 + 1863i$	$-113 + 1857i$	$-117 + 1857i$	$-77 + 1562i$	$-77 + 1562i$
10	$-215 + 2613i$	$-160 + 2246i$	$-161 + 2247i$	$-122 + 1858i$	$-126 + 1856i$
11	$-233 + 2719i$	$-326 + 2745i$	$-411 + 2764i$	$-161 + 2247i$	$-161 + 2248i$
12	$-260 + 2870i$	$-544 + 3287i$	$-545 + 3459i$	$-490 + 2805i$	$-552 + 2868i$

All presented eigenvalues has been calculated for 2000 rpm and for nozzle excitation with thirty fold times higher frequency than disc speed.

rotates, stiffening effects under rotation increase and values of natural frequencies increase too, except the lowest one. Mode shapes and natural frequencies under rotation are moreover influenced by the lock-effect, which is caused by centrifugal forces acting on friction element. After locking, blade shrouds are interconnected as if they are one rigid element and between the friction areas the micro-slip motion appears only.

3.1.2. Nonconservative model

Taking into account the influence of contact and friction damping, number of complex eigenvalues vanishes and real eigenvalues appear instead. This is the desired positive effect of friction damping because corresponding mode shapes are also super-critically damped. This effect can be clearly seen in Table 2, where first twelve eigenvalues are presented for different contact friction coefficients. For example, if friction coefficient $f = 0.2$ and rotational speed is 2000 rpm, we have 47 complex conjugate eigenvalues and 62 negative real eigenvalues. The number of complex and real eigenvalues changes slightly along with rotational speed of the disc. Further, because of the influence of matrices of softening and bending stiffening under rotation and because of the coupling friction effects, imaginary parts of eigenvalues depend not only on rotational speed but also on excitation frequency. This effect can be clearly seen in Fig. 5, where imaginary parts of first ten eigenvalues are plotted in dependence on rotational speed of the disc. The straight line corresponds to dependence of excitation with frequency thirtyfold higher than rotational frequency of the disc. This case corresponds to undermentioned considered excitation frequency. Further, it is worthy to be noticed here that the considered excitation is defined in (30) and it acts in axial direction of the disc. Therefore, imaginary parts of eigenvalues corresponding to mode shapes dominantly vibrating in axial direction are influenced only (i.e. the fourth, the sixth, the eighth and the tenth mode). As an illustration, in Fig. 6, chosen mode shapes are plotted considering damped model ($f = 0.2$) rotating with rotational velocity of 2000 rpm.

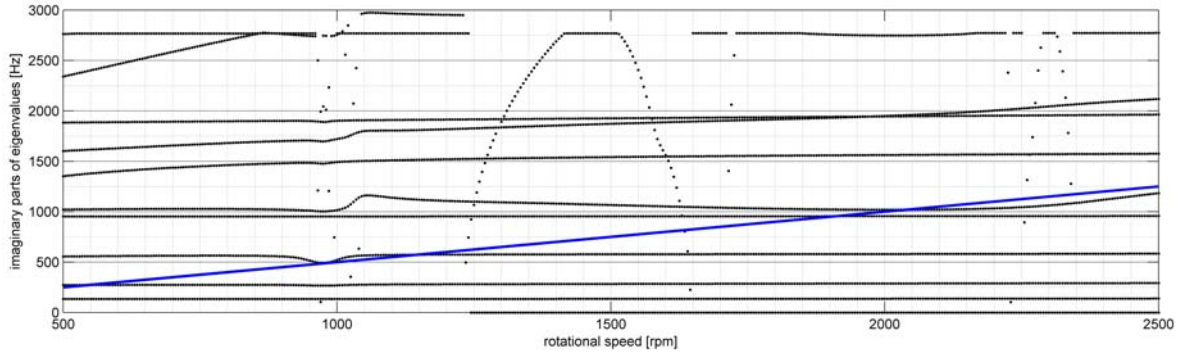


Fig. 5. Dependence of imaginary parts of eigenvalues on rotational speed of the disc and on excitation frequency

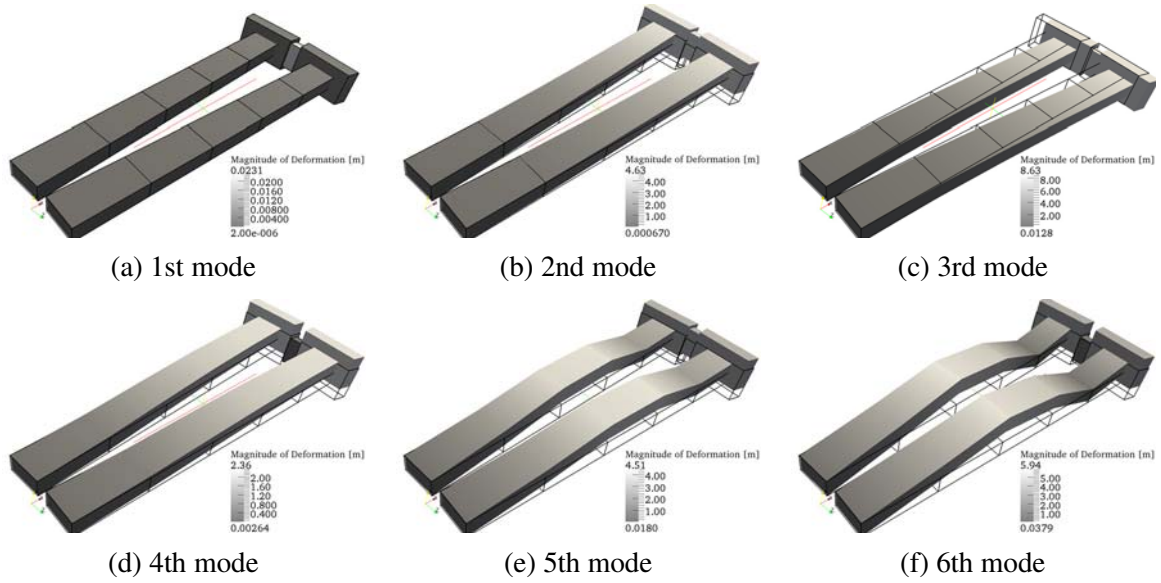


Fig. 6. Chosen mode shapes corresponding to damped model

3.2. Steady-state response to external excitation

The model derived above was used for determination of steady-state response to arbitrary harmonic component of periodic excitation with frequency corresponding to angular velocity ω of the disc. The excitation considered here simulates electromagnetic pulses acting on the blade shroud. The electromagnets are placed in the fixed nonrotating system and act on the blades at an instant of blade passage around the electromagnet (see Fig. 4). Since the blades rotate with constant angular velocity ω , the electromagnetic pulses acting on each blade are mutually delayed by $\Delta t = \frac{2\pi}{\omega n_B}$, where n_B denotes number of blades uniformly distributed around the circumference of the rotating disc. By the reason that the excitation regarding bladed disc is periodic with basic frequency equal to rotational frequency of the disc, the vector of complex amplitudes of external periodic excitation in (24) can be determined using Fourier series with the first K terms in following form

$$\mathbf{f}(\omega, t) = [\dots, 0, \dots, e^{-i\omega\Delta t}, \dots, 0, \dots, 1, \dots, 0, \dots]^T \sum_{k=1}^K F_k e^{ik\omega t}, \quad F_k = F_0/k, \quad (30)$$

where the two nonzero elements denote complex amplitudes of excitation with fundamental frequency ω and correspond to coordinates describing axial displacements (in direction of rotation axis) of nodes C_1 and C_2 of both blade shrouds. The excitation of the first blade is time-shifted about Δt which designates the time between passage of blades around the electromagnet. Based on the periodic excitation (30), the steady state response can be calculated for each harmonic component of excitation.

3.3. Steady-state calculation procedure

The calculation procedure of steady-state response of two blades with shroud can be summarized as follows:

1. Creation of the model of blade couple with friction element considering material damping only and neglecting both friction forces in contact planes ($f = 0$), i.e. determining the matrices in (7).
2. Contact stiffness and damping matrices determination according to (8)–(14) and further detail described in Appendices A and B.
3. Mathematical model creation without friction forces effects.
4. Steady-state response calculation for given harmonic excitation (24) without friction forces effects.
5. Calculation of complex slip amplitudes of steady-state harmonic motion according to (25)–(28) in contact points A and B .
6. Determination of coefficients of equivalent viscous translational and rotational damping (18) using absolute values of complex slip amplitudes in contact points A and B .
7. Composition of equivalent damping matrix based on equivalent viscous coefficients.
8. More accurate steady-state response calculation for given harmonic excitation considering the equivalent viscous friction damping.

Following above mentioned eight steps one can get steady-state response of a blade couple considering the friction effects in the blade shroud. Steps 4 to 8 can be used as an iteration process when the steady-state response from step 8 is chosen to be an initial condition for the second and the later iterations. In the next, presented results have been gained using the first iteration only because the iteration process do not converge due to the equivalent damping coefficients expression (18). The point is that taking into account the equivalent damping coefficient, the steady-state response decreases along with slip amplitudes and therefore the equivalent damping coefficient increases. Also, this approach can serve as a first approximation of the nonlinear model solution only.

As an illustration, in Fig. 7 absolute values of complex amplitudes of translational displacements of the first blade shroud are plotted in dependence on rotational speed for $k = 30$ and $F_0 = 100$ N. The friction coefficients of both friction surfaces are equal $f_a = f_b$. The considered harmonic part of excitation corresponds to nozzle frequency ($k = n_B$). Then resonant speeds $n_{\nu,k} = 60/k\text{Im}\{f_{\nu}\}$ rpm in given speed range correspond to ν -th natural frequency excited by k -th harmonic component of excitation.

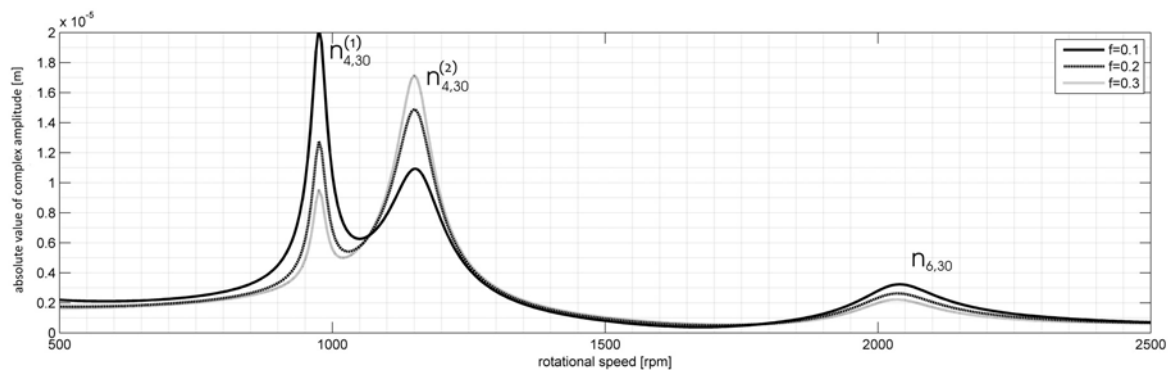


Fig. 7. Absolute values of complex amplitudes of translational displacement of the first blade shroud in direction of rotation axis for different friction coefficients

One can see three resonant peaks in Fig. 7 corresponding to the fourth and to the sixth natural frequency, $n_{4,30}^{(1)} = 980$ rpm, $n_{4,30}^{(2)} = 1150$ rpm and $n_{6,30} = 2045$ rpm. Taking into account the mode shapes plotted in Fig. 6 and the axial direction of excitation, the resonant frequencies coincide with natural frequencies corresponding to bending mode shapes in xy plane. The first two peaks correspond to the fourth frequency because of the dependence of imaginary parts of eigenvalues on rotational speed and on excitation frequency. Comparing Fig. 5 and Fig. 7 the leading line intersects the fourth frequency in two points. Changing the friction coefficient, the values of fourth frequency draw apart the leading line in the area of first resonant peak. And that is the reason why the first peak is less dominant for higher values of friction coefficient.

4. Conclusion

This paper presents a method focused on modelling of friction effects in blade shroud which are realized by means of friction elements placed in between the blade shroud. A model of two rotating blades with shroud is derived and can be easily generalized for complete bladed disc as well as the developed methodology for linearization of nonlinear friction forces acting between the blades and the friction element. The first gained results confirm that the efficiency of friction forces is dominant in resonant states. The linearization of friction forces is based on the harmonic balance method which is used for equivalent damping coefficients determination in dependence on the amplitudes of relative slip motion between blades and the friction element. According to the methodology the in-house software in MATLAB was created and tested on a model of two rotating blades with shroud.

Acknowledgements

This work was supported by the GA CR project No. 101/09/1166 “Research of dynamic behaviour and optimization of complex rotating systems with non-linear couplings and high damping materials”.

References

- [1] Allara, M., A model for the characterization of friction contacts in turbine blades, *Journal of Sound and Vibration* 320 (2009) 527–544.

- [2] Borrajo, J. M., Zucca, S., Gola, M. M., Analytical formulation of the Jacobian matrix for non-linear calculation of forced response of turbine blade assemblies with wedge friction dampers, *International Journal of Non-Linear Mechanics* 41 (2006) 1 118–1 127.
- [3] Cha, D., Sinha, A., Statistics of responses of a mistuned and frictionally damped bladed disk assembly subjected to white noise and narrow band excitations, *Probabilistic Engineering Mechanics* 21 (2006) 384–396.
- [4] Cigeroglu, E., An, N., Menq, C. H., A microslip friction model with normal load variation induced by normal motion, *Nonlinear Dynamics* 50 (2007) 609–626.
- [5] Csaba, G., Forced response analysis in time and frequency domains of a tuned bladed disk with friction dampers, *Journal of Sound and Vibration* 214 (3) (1998) 395–412.
- [6] Firrone, C. M., Zucca, S., Underplatform dampers for turbine blades: The effect of damper static balance on the blade dynamics, *Mechanics Research Communications* 36 (2009) 515–522.
- [7] Kellner, J., Vibration of turbine blades and bladed disks, Ph.D. thesis, University of West Bohemia, Pilsen, 2009. (in Czech)
- [8] Byrtus, M., Hajžman, M., Zeman, V., Dynamics of rotating systems, University of West Bohemia, Pilsen, 2010. (in Czech)
- [9] Nayfeh, A. H., Mook, D. T., *Nonlinear oscillations*, Wiley-VCH Verlag, Weinheim, 2004.
- [10] Půst, L., Veselý, J., Horáček, J., Radolfová, A., Research on friction effects in blades model, Institute of Thermomechanics, Academy of Sciences of the Czech Republic, Prague, 2008. (research report, in Czech)
- [11] Půst, L., Horáček, J., Radolfová, A., Beam vibration with a friction surface on perpendicular extenders, Institute of Thermomechanics, Academy of Sciences of the Czech Republic, Prague, 2008. (research report, in Czech)
- [12] Rivin, E. I., *Stiffness and damping in mechanical design*, Marcel Dekker, New York, 1989.
- [13] Schmidt-Fellner, A., Siewert, C., Panning, L., Experimental analysis of shrouded blades with friction contact, *Proceedings in Applied Mathematics and Mechanics* 6 (2006) 263–264.
- [14] Tokar, I. G., Zinkovskii, A. P., Matveev, V. V., On the problem of improvement of the damping ability of rotor blades of contemporary gas-turbine engines, *Strength of Materials* 35 (4) (2003) 368–375.
- [15] Toufine, A., Barrau, J. J., Berthillier, M., Dynamics study of a structure with flexion-torsion coupling in the presence of dry friction, *Nonlinear Dynamics* 18 (1999) 321–337.
- [16] Rao, S. S., *Mechanical vibrations (Fourth Edition)*, Pearson Prentice Hall, 2004.
- [17] Zeman, V., Kellner, J., Modelling of vibration of moving blade packet, *Modelling and Optimization of Physical systems, Zeszyty naukowe* 31 (2006), 155–160, Gliwice.

Appendix A — Contact stiffness

Let us summarize the determination of contact stiffnesses. The contact stiffnesses can be determined based on expression of contact forces and contact torques transmitted by contact surfaces. As the first step, let us express the torques caused by contact forces, which are acting at friction element by supposed centric placed rectangular effective surfaces a and b , can be expressed under assumption of constant surface stiffnesses $\kappa_a = k_a / (h_{aef} a_{ef})$, $\kappa_b = k_b / (h_{bef} b_{ef})$ along the whole contact area. Using this assumption, torques of contact forces, e.g. in surface b , can be expressed in local coordinate system ξ_B, η_B, ζ_B (see Fig. 8) under assumption of relative angular displacements $\varphi_{\xi_B}, \varphi_{\eta_B}, \varphi_{\zeta_B}$ of friction element (surface b) around axes ξ_B, η_B, ζ_B with

respect to the shroud as

$$M_{\xi_B}^{(b)} = 2 \int_0^{h_{bef}/2} \underbrace{\kappa_b b_{ef} d\eta}_{dN} \underbrace{\eta \varphi_{\xi_B}}_{\text{deformation}} \eta = \frac{1}{12} \underbrace{\kappa_b b_{ef} h_{bef}}_{k_{\zeta_B}} h_{bef}^2 \varphi_{\xi_B} = k_{\xi_B \xi_B}^{(b)} \varphi_{\xi_B},$$

$$M_{\eta_B}^{(b)} = 2 \int_0^{b_{ef}/2} \underbrace{\kappa_b h_{bef} d\xi}_{dN} \underbrace{\xi \varphi_{\eta_B}}_{\text{deformation}} \xi = \frac{1}{12} \underbrace{\kappa_b b_{ef} h_{bef}}_{k_{\zeta_B}} b_{ef}^2 \varphi_{\eta_B} = k_{\eta_B \eta_B}^{(b)} \varphi_{\eta_B}.$$

Based on the placement of the coordinate system ξ_B, η_B, ζ_B , there appears no contact force by rotational motion around the ζ_B axis which is perpendicular to the surface b . Therefore, corresponding contact torque is zero too

$$M_{\zeta_B}^{(b)} = 0.$$

Linearized rotational contact stiffnesses in surface b with respect to axes ξ_B, η_B, ζ_B of friction element result from above given terms, i.e.

$$k_{\xi_B \xi_B}^{(b)} = \frac{1}{12} k_{\zeta_B} h_{bef}^2, \quad k_{\eta_B \eta_B}^{(b)} = \frac{1}{12} k_{\zeta_B} b_{ef}^2, \quad k_{\zeta_B \zeta_B}^{(b)} = 0.$$

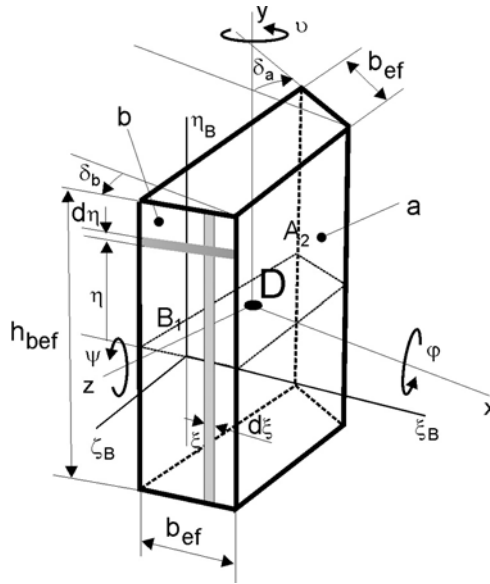


Fig. 8. Friction element detail

Derived contact stiffnesses are expressed in coordinate systems connected with contact surfaces. To express contact forces acting on friction element and blade ends, these forces has to be transformed in proper coordinate systems.

Appendix B — Contact forces and structure of contact matrices

In contact points B_1, A_2 placed between blade shrouds and friction element, contact elastic forces and torques are acting. These force effects are transformed into blade end points C_1 and

C_2 and into the center of mass D of friction element. In configuration space of generalized coordinates $\mathbf{q} \in \mathbb{R}^{6(N_1+1+N_2)}$, where N_1 and N_2 are numbers of blade nodes, vector of elastic couplings forces can be expressed in the form

$$\mathbf{K}_C \mathbf{q} = [\dots, \mathbf{f}_{C_1}^T, \mathbf{m}_{C_1}^T, \mathbf{f}_a^T + \mathbf{f}_b^T, \mathbf{m}_a^T + \mathbf{m}_b^T, \dots, \mathbf{f}_{C_2}^T, \mathbf{m}_{C_2}^T]^T. \quad (31)$$

Vectors \mathbf{f}_{C_1} , \mathbf{f}_{C_2} and \mathbf{m}_{C_1} , \mathbf{m}_{C_2} represent forces and torques by which friction element acts on blades in nodes C_1 and C_2 . Vectors \mathbf{f}_a , \mathbf{f}_b and \mathbf{m}_a , \mathbf{m}_b express forces and torques, respectively, by which the shrouds act on friction element in mass center D . Particular vectors have nonzero components regarding axes x_j, y_j, z_j ($j = 1, 2$) and x, y, z .

Let us express particular forms of force and torque vectors presented in equation (31). Vectors \mathbf{f}_{C_1} and \mathbf{m}_{C_1} express effects of friction element on the blade in node C_1 . These vectors are expressed in coordinate system x_1, y_1, z_1 where the origin is identical to point C_1 . Vector \mathbf{f}_{C_1} includes effects of normal and friction forces acting at the blade in contact point B_1 and have following form

$$\mathbf{f}_{C_1} = \begin{bmatrix} -N_{B_1} \sin \delta_B + T_{B_1\xi} \cos \delta_B \\ T_{B_1\eta} \\ -N_{B_1} \cos \delta_B - T_{B_1\xi} \sin \delta_B \end{bmatrix}.$$

Symbols $T_{B_1\xi}$ and $T_{B_1\eta}$ represent ξ - and η -components of friction force T_{B_1} . Further, the vector expressing the torque can be expressed as follows

$$\mathbf{m}_{C_1} = \mathbf{R}_{B,C_1} \mathbf{f}_{C_1},$$

where $\mathbf{R}_{B,C_1} \in \mathbb{R}^{3,3}$ is a matrix of vector product and has following antisymmetric structure

$$\mathbf{R}_{B,C_1} = \begin{bmatrix} 0 & -z_{B_1} & y_{B_1} \\ z_{B_1} & 0 & 0 \\ -y_{B_1} & 0 & 0 \end{bmatrix}. \quad (32)$$

Nonzero elements in the term above represent coordinates of contact point B_1 in coordinate system x_1, y_1, z_1 . Let us follow next terms in equation (31). The vector \mathbf{f}_a represents force effect of the blade shroud acting on friction element in the surface a with the centre A_2 and it has following form

$$\mathbf{f}_a = \begin{bmatrix} -N_{A_2} \sin \delta_a + T_{A_2\xi} \cos \delta_a \\ T_{A_2\eta} \\ N_{A_2} \cos \delta_a + T_{A_2\xi} \sin \delta_a \end{bmatrix}.$$

Similarly, the vector \mathbf{f}_b has the form

$$\mathbf{f}_b = \begin{bmatrix} -N_{B_1} \sin \delta_b + T_{B_1\xi} \cos \delta_b \\ T_{B_1\eta} \\ -N_{B_1} \cos \delta_b - T_{B_1\xi} \sin \delta_b \end{bmatrix}.$$

Corresponding torques acting on the friction element can be expressed similarly as above

$$\mathbf{m}_a = \mathbf{R}_{A,D} \mathbf{f}_a, \quad \mathbf{m}_b = \mathbf{R}_{B,D} \mathbf{f}_b.$$

Matrices $\mathbf{R}_{A,D}$ and $\mathbf{R}_{B,D}$ have the structure as shown in (32). Vectors \mathbf{f}_{C_2} and \mathbf{m}_{C_2} are then expressed following the same steps as above using corresponding values.

It is efficient to split their expression to translational contact deformations in dependence on translational contact stiffnesses k_a, k_b , rotational contact deformations in dependence on rotational contact stiffnesses derived in Appendix A and to axial contact deformation in dependence on axial mounting stiffnesses $k_{ax}^{(a)}$ and $k_{ax}^{(b)}$ of friction element in blade shroud. Therefore, the vector of elastic coupling forces can be written in separated form

$$\mathbf{K}_C \mathbf{q} = \left(\mathbf{K}_C^{(t)} + \mathbf{K}_C^{(r)} + \mathbf{K}_C^{(ax)} \right) \mathbf{q},$$

to which the coupling matrix (14) corresponds. Structure of these matrices is given below, where crosshatch blocks designate nonzero block matrices of order 6 as well as the dimension of vectors of generalized coordinates of corresponding nodes.

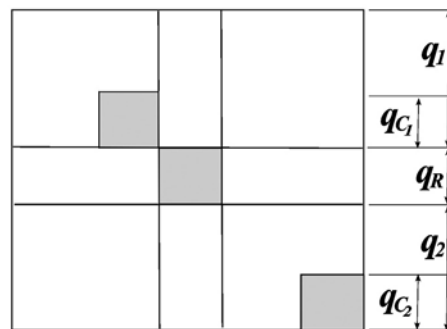


Fig. 9. Coupling stiffness matrices